 DOI: 10.1002/masy.201050407

Isothermal and Non-Isothermal Crystallization Kinetics and Morphology of Poly(trimethylene terephthalate)/Multiwalled Carbon Nanotube Composites

*Anju Gupta, Veena Choudhary**

Summary: Multiwalled carbon nanotubes (MWCNTs) synthesized using chemical vapor deposition method were dispersed in poly(trimethylene terephthalate) (PTT, Mv = 88,000) by melt compounding technique using DMS microcompounder. The nanocomposites consisting of varying amounts of MWCNTs were characterized by differential scanning calorimetry (DSC), wide-angle X-ray diffraction (WAXD), Raman spectroscopy, scanning electron microscopy (SEM) and transmission electron microscopy (TEM). The effect of carbon nanotubes on the crystallization behavior (under isothermal and non isothermal crystallization conditions) of PTT was studied using DSC. The presence of carbon nanotubes didn't show any significant effect on crystallization temperature of PTT matrix under non-isothermal conditions. Crystallization studies under isothermal conditions were carried out at different temperatures i.e 185, 190, 195 and 200 °C. Complete crystallization was observed within 60 sec at 185 °C whereas at 200 °C, longer time was required for complete crystallization. Crystal growth was also investigated using hot stage polarizing microscope (PLM). The effect of annealing time at 200 °C was investigated in the presence as well as in the absence of varying amounts of MWCNTs. Spherulitic growth was seen and the spherulite size in all the samples increased with annealing time. Morphological characterization using SEM and TEM showed a uniform dispersion of MWCNTs and poor compatibility with PTT matrix.

Keywords: crystallinity; multiwalled carbon nanotubes; nanocomposites; nucleation; poly(trimethylene terephthalate)

Introduction

Poly(trimethylene terephthalate) [PTT] is an aromatic polyester with odd number of methylene units in the glycol moiety of its chemical repeat unit. The first patent on PTT synthesis was presented early in the 1940s, using dimethyl terephthalte and 1, 3-propane diol. However, due to the high cost of the starting raw material 1,3-propane diol, further development of PTT was baffled for quite a long time. PTT has become commercially viable in 1990s, with a breakthrough in the synthesis of 1, 3-propanediol.[1]

PTT is semicrystalline polyester like poly(ethylene terephthalate) [PET] and poly(butylene terephthalate) [PBT]. PTT was found to have high elastic recovery and resilience as an engineering plastic and has mechanical properties comparable to PET while its processing characteristics are similar to PBT.[2–4] With such a blend of properties, PTT seems to be a promising raw material for engineering applications.

Recently to explore the application area of PTT, various nano fillers have been

Centre for Polymer Science and Engg., Indian Institute of Technology Delhi, Hauz Khas, New Delhi 110016, India
Fax: 011-26591421; E-mail: veenach@hotmail.com

incorporated into the polymer. Their main advantage over traditional reinforcements comes from their high aspect ratio and associated high surface-area-to-volume ratio [5]. Incorporation of clay into the PTT matrix improved its mechanical properties, thermal stability and crystallization rate.[6–9] Very recently, owing to extraordinarily high mechanical strength and excellent electrical/thermal conductivity, carbon nanotubes (CNT) has become the next-generation reinforcements for nano structured polymeric composite materials. Although incorporation of CNT in polyester matrix [PET/PBT/PTT] by melt compounding, solution blending or in- situ polymerization has been reported in the literature[10–18] and investigated its effect on thermal, mechanical and electrical properties of polymer. Crystallization behavior of PET and PBT has also been investigated in the presence of CNTs but to the best of our knowledge, only one paper reported the crystallization behavior of PTT in presence of modified CNTs.[19] As it is well reported that the modification causes some change in properties of CNTs which inturn will affect the crystallization behavior. Therefore the study of crystallization behavior of PTT in presence of pure CNTs is important to explore full potential applications of carbon nanotubes. In this paper, we reported the crystallization behavior under isothermal and non-isothermal conditions and morphology [Raman, WAXD, SEM and TEM] of PTT/MWCNT nano-composites in the presence of varying amounts of CNTs.

Experimental Part

Poly(trimethylene terephthalate) [PTT] pellets were procured from Futura Polymers (Chennai, India). The intrinsic viscosity of polymer was determined in 3:2 phenol: 1,1,2,2-tetrachloroethane at 30 °C and found to be [η] 1.29V dL/g. The molecular weight determined using Mark –Houwink equation $\{[\eta] = KMv^{\alpha}\}$ was found to be 88000. The value of K and α was taken from the literature as 5.36×10^{-4} g/dL and 0.69 respectively.[20]

Carbon nanotubes were synthesized by using chemical vapor deposition (CVD) method. About 8% ferrocene dissolved in toluene was used as a source of Fe catalyst and hydrocarbon. A conventional two zone reactor was used. The reactor zone was maintained at 350 °C and 750 °C. Once the temperature was reached, the solution containing a mixture of ferrocene and toluene was injected in the quartz reactor. Argon was also fed along with the raw materials as a carrier gas and its flow rate was adjusted so that the maximum amount of precursor is consumed in the high temperature zone. Carbon nanotubes deposited on the inside wall of the quartz reactor were harvested and its purity and structural characterization was done using thermogravimetry, scanning electron microscopy and Raman spectroscopy.

PTT/MWCNT nanocomposites were prepared by melt mixing using co-rotating DMS micro-5 compounder. The polymer and CNTs was vacuum dried overnight at 100 °C before compounding. Compounding was done at a temperature of 265 °C for 5 minutes at a screw speed of 170 rpm. Nanocomposites were prepared by mixing varying amounts of MWCNTs i.e 0.5, 1 and 2% w/w with PTT. After melt compounding, the strands of nanocomposites were manually cut to small pellets for further processing. After the melt compounding, the samples for testing were prepared by compression molding [260 °C for 5 minutes at a pressure of 4400 lb in an electrically heated Carver hydraulic press].

Perkin Elmer Pyris 6 Differential Scanning Calorimeter (DSC) was used for recording DSC scans (heating and cooling) under N_2 atmosphere for isothermal and non-isothermal crystallization studies. About 5–6 mg of samples was first heated from room temperature to 260 °C at a heating rate of 10 °C/min and then held at that temperature for 5 minutes to remove the thermal history of the material. The sample was then cooled to 35 °C at a cooling

rate of 10 °C/min and again heated to 260 °C at the same rate.

To investigate the crystallization behavior of PTT and PTT/MWCNT composite samples under isothermal conditions, the samples were heated from room temperature to 260 °C at a heating rate of 10 °C/min, held for 5 min at that temperature to eliminate thermal history and then quickly cooled to the predetermined crystallization temperatures 185 °C, 190 °C, 195 °C and 200 °C. The DSC scans were then recorded as a function of time.

The thermal behavior of PTT and PTT/MWCNT nanocomposites under non-isothermal conditions was investigated by heating the samples to 260 °C at a heating rate of 10 °C/min, held at 260 °C for 5 minutes to eliminate thermal history and then cooled to room temperature at a cooling rate of 5,10,15 and 20 °C/min. The DSC scans were then recorded as a function of temperature.

Hot stage polarizing microscope (Meize Techno Japan) was used to observe the morphology of film samples under isothermal crystallization temperature. Specimens were prepared by melting the PTT films on a glass slide at 260 °C, followed by pressing the melt samples with a piece of cover glass and held for 5 min to remove the thermal history. Then the samples were rapidly quenched to the predetermined crystallization temperature. The subsequent growth of particularly selected PTT crystals was recorded by a video camera at appropriate time intervals.

Morphological characterization was done using EVO-50 scanning electron microscope (SEM). For morphological characterization, manually fractured compression molded samples were used. The samples were coated first with silver by a silver sputtering device and then micrographs were taken at a magnification of 15 KX.

Transmission electron microscopy (TEM) images were obtained using a JEOL 2100F TEM microscope operated at an accelerating voltage of 200 kV to observe the nanoscale structure of MWCNT and the PTT/MWCNT nanocomposites. Ultra-thin sections 30–80 nm of nano-composites were prepared using Leica Ultamicrotome.

Wide angle X-ray diffraction (WAXD) patterns were recorded on a PANatytical instrument, model number PW3040/60 X'pert PRO (Netherlands), using Ni filtered CuKα radiation ($\lambda = 0.154$ nm). The voltage and the current of X-ray were 40 KV and 30 mA respectively. The samples were scanned at a rate of 2°/min from 2° to 70° of 2θ. Samples obtained after compression molding were used for recording X-ray diffraction patterns.

Raman spectrometer (Renishaw InVia Raman microscope) was used to evaluate the structure and crystallinity of PTT and PTT/MWCNT composites. For Raman studies, film samples were used. These spectra were recorded using diode laser at 785 nm excitation with Raman shift between 100 cm^{-1} -3000 cm^{-1}.

Results and Discussion

The purity of MWCNTs was determined from thermogravimetric analysis (TGA) under oxygen atmosphere. A constant supply of dry air flow rate = 10 ml/min was maintained as the temperature was raised from room temperature to 1000 °C. The TG/DTG trace for CNT shown in Figure 1 suggests that there is no mass loss up to 500 °C, after which a sharp mass loss was observed with the DTG peak at 550 °C. The mass loss in this region is due to the oxidation of MWCNTs present in the sample. Absence of any mass loss in the low temperature region i.e. between 300 and 400 °C suggests the absence of amorphous carbon in the sample.[21] No mass loss was observed beyond 600 °C. The total mass loss up to 1000 °C was ~88% due to oxidation or burn out of carbon nanotubes. The remaining 12% char could, therefore, be due to either iron catalyst or its oxide present in the sample as impurity.

SEM micrographs of CNTs [Figure 2(a)] show large bundles of carbon nanotubes with a diameter in the range of 30–40 nm

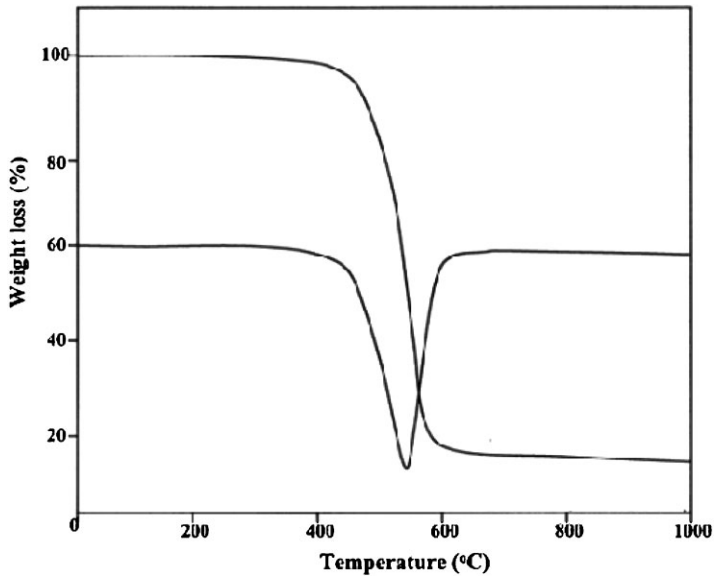

Figure 1.
TG/DTG trace of MWCNTs.

and nearly 20–30 μm in length. The transmission electron micrograph shown in [Figure 2(b)] was taken on Philips CM-12. The micrographs show that carbon nanotubes are multiwalled with varying inner diameter (10 to 12 nm) and outer diameter from 30 to 40 nm. Micrographs also confirm the presence of small amount of catalyst encapsulated in the tube.

Room temperature Raman scattering studies of CNT [Figure 13] shows the characteristic tangential band at 1580 cm^{-1} (G band) and the disorder-induced band at 1352 cm^{-1} (D band).[22] Raman scattering studies were performed using an Ar ion laser (514.5 nm excitation) and an ISA Triax 550 single grating spectrometer. All Raman scattering data were collected in the back scattering geometry.

Thermal behavior of PTT/MWCNT composites was investigated by recording DSC scans at a cooling rate of 10 °C/min. Figure 3 show the DSC scans of PTT in the absence and presence of varying amounts of CNTs. An exothermic transition due to crystallization was seen in all the samples. The crystallization exotherm was characterized by noting the onset of crystallization (T_{onset}), peak exothermic temperature

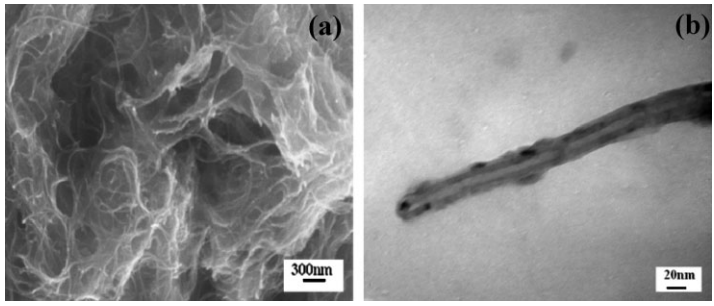

Figure 2.
Images of MWCNTs (a) Scanning electron microscopy (b) Transmission electron microscopy.

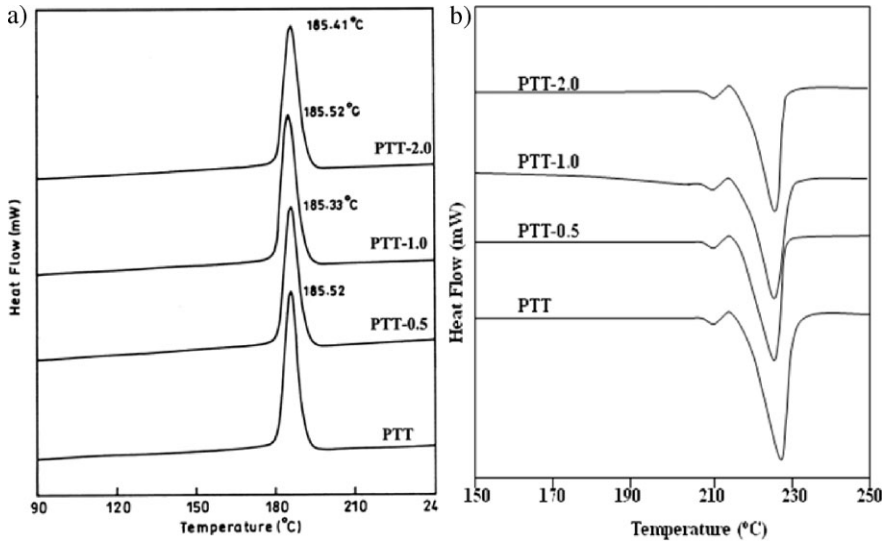

Figure 3.
DSC scans of PTT/MWCNT nanocomposite (a) cooling and (b) heating scans.

(T_{exo}) and end set temperature (T_{end}). From the area under the exotherm, heat of crystallization was calculated and the results are summarized in Table 1.

Second heating scans were used to evaluate the melting characteristics of PTT in the absence and presence of varying amounts of CNTs. Two melting endotherms were seen in all the samples. The occurrence of first small melting endotherm is attributed to recrystallization during the re-heating process and second melting endotherm to the melting of primary crystallites of PTT.[23–24] From the melting endotherm, peak endotherm temperature (T_m) and heat of fusion (ΔH_f) was determined and the results are given in Table 2. From the knowledge of heat of fusion, % crystallinity was calculated using the following equation.

$$Xc(\%) = H_f/H_{fo} \times 100 \quad (1)$$

H_{fo} is heat of fusion for 100% crystalline PTT which is taken as 146 J/g from the literature.[25] The results of cooling and heating scans are summarized in Table 1

Table 1.
Results of DSC scans (Cooling): effect of MWCNTs on crystallization behavior of PTT.

Sample Designation	T_{onset} (°C)	T_{exo} (°C)	T_{end} (°C)	ΔH_c (J/g)
PTT	190.7	185.5	162.7	50.6
PTT-0.5	191.4	185.3	168.4	49.4
PTT -1.0	191.4	185.5	168.0	49.4
PTT -2.0	191.0	185.4	170.3	49.0

Table 2.
Results of DSC scans (Heating): effect of MWCNTs on melting behavior and percent crystallinity of PTT.

Sample Designation	First Endotherm		Second Endotherm		ΔH_f (J/g)	Crystallinity (%)
	T_o (°C)	T_{m1} (°C)	T_o' (°C)	T_{m2} (°C)		
PTT	204.0	210.2	218.2	225.0	50.6	35.1
PTT-0.5	204.8	210.7	218.3	225.8	49.4	34.2
PTT-1.0	204.4	210.3	218.0	225.4	49.4	34.1
PTT-2.0	204.3	210.3	218.2	225.5	49.0	34.5

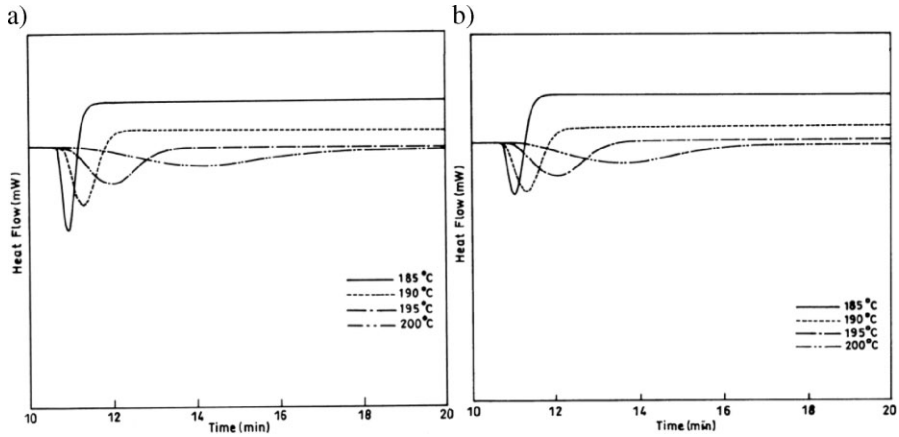

Figure 4.
Isothermal crystallization exotherms of PTT/MWCNT nanocomposites at various crystallization temperatures (a) PTT (b) PTT-1.0.

and 2. The onset of crystallization, peak exotherm temperature and melting endotherm peak temperature as well as percent crystallinity of PTT remained unaffected upon incorporation of varying amounts of CNTs, indicating that CNTs are not acting as nucleating agent.

Isothermal and non-isothermal crystallization behavior of PTT/MWCNT composites was investigated using DSC. Figure 4 shows the isothermal crystallization exotherms of pure PTT as well as PTT/MWCNT nanocomposites at different crystallization temperatures. As the crystallization temperature increased, the exothermic peak shifted to longer time, implying that the crystallization rate decreased with the increasing crystallization temperature.

The well known Avrami equation [Eq. 2] is the most commonly used approach to study isothermal crystallization process of polymers.[26]

$$1 - X_t = \exp(-kt^n) \quad (2)$$

Where 'n' is the Avrami exponent and gives information about the type of nucleation and crystal growth, k the Avrami rate constant and X_t the relative crystallinity at time t. Figure 5 show the change in relative crystallinity (X_t) of PTT with time (t). It was found that X_t increases with the

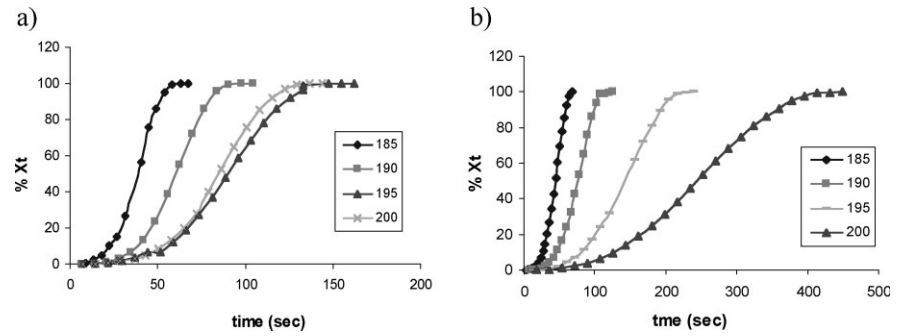

Figure 5.
Plot of Xt vs. t for of PTT/MWCNT nanocomposites at various crystallization temperatures (a) PTT (b) PTT-1.0.

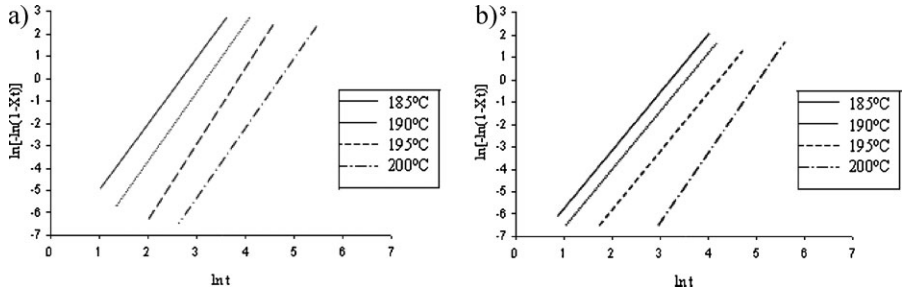

Figure 6.
Plot of ln[-ln(1-Xt)] vs. ln t in PTT and PTT/MWCNT nanocomposite at various crystallization temperatures (a) PTT (b) PTT-1.0.

increase of time. Using Eq. (2) in double logarithmic form

$$\ln[-\ln(1-X_t)] = \ln k + n \ln t \qquad (3)$$

and plotting ln [-ln (1-X_t)] vs. ln t, a straight line is obtained, and the value of 'n' and k can be directly obtained from the slope and intercept of the best fitted lines, as shown in Figure 6. The half time of crystallization i.e. $t_{1/2}$ was also calculated and the values of n, k, and $t_{1/2}$ are given in Table 3.

For pure PTT the Avrami exponent, 'n' was found to be 2.4–2.7 at different crystallization temperatures. The Avrami exponent increased slightly upon incorporation of MWCNTs and found to be in the range of 2.4–3.3. The value of 'n' for neat PTT indicates a three dimensional spherulitic growth, indicating heterogeneity in the process, because the theoretical value of 'n' should be 4.0 for three dimensional growths with homogeneous nucleation. This may be attributed to the presence of polymerization catalyst which can act as heterogeneous nucleating agent in the crystallization process. However incorporation of MWCNTs in PTT matrix increases 'n' value and resulted in a decrease in the heterogeneity except at higher temperature. These results indicate that the incorporation of MWCNTs have altered the mechanism of nucleation and crystal growth of PTT. This also shows that MWCNTs are not acting as nucleating agent but hindering the chain mobility of polymer at lower crystallization temperature. Therefore in presence of nanotubes number of nucleating sites decreases as well

Table 3.
Isothermal crystallization kinetic parameters of PTT/MWCNT nanocomposites.

Sample Designation	Crystallization Temperature (°C)	n	k/sec^{-n}	$t_{1/2}$/sec
PTT	185	2.7	1.30×10^{-4}	23
	190	2.6	7.38×10^{-5}	32
	195	2.4	3.32×10^{-5}	65
	200	2.6	7.30×10^{-7}	186
PTT-0.5	185	2.7	1.26×10^{-4}	24
	190	2.8	2.37×10^{-5}	36
	195	2.8	3.72×10^{-6}	69
	200	2.5	1.75×10^{-6}	169
PTT-1.0	185	2.4	3.88×10^{-4}	21
	190	2.5	1.26×10^{-4}	32
	195	2.6	1.22×10^{-5}	65
	200	3.1	7.54×10^{-8}	166
PTT-2.0	185	2.5	2.31×10^{-4}	24
	190	2.8	2.32×10^{-5}	36
	195	2.5	1.63×10^{-5}	71
	200	2.8	4.70×10^{-7}	142

as rate of crystal growth decreases. Similar behavior has been reported by Kim et al. in poly(ethylene naphthalate) [PEN]/ SWCNT system.[27]

The results of half crystallization time $t_{1/2}$ and rate constant k listed in Table 3, show slower rate of crystallization in the presence of CNTs as compared to neat PTT. With increase in MWCNTs loading, however, $t_{1/2}$ increases gradually at lower temperature. This is an indicative of a decrease in crystallization rate. This decrease in $t_{1/2}$ is attributed to the high melt viscosity of polymer at a temperature lower than its melting temperature, which does not allow the PTT chains to be aligned. A different behaviour was observed at a temperature of 200 °C i.e. close to its melting temperature, where the PTT chains have sufficient chain mobility to form crystal and $t_{1/2}$ decreased gradually with increase in MWCNTs loading, indicating a monotonous increase in the crystallization rate reflecting that at higher temperature melt viscosity is lower therefore PTT chains can be easily aligned or in other words CNTs enhances the crystallisation rate.

In the non-isothermal crystallization process, the time t has the following relation with temperature T (Eq.4) and the relative crystallinity (X_t) as a function of crystallization temperature is deduced by

$$t = T_0 - T/C \tag{4}$$

$$X_t = \frac{\int_{T_0}^{T} \frac{dH}{dt} dt}{\int_{T_0}^{T_{00}} \frac{dH}{dt} dt} \tag{5}$$

Where T_0 is initial temperature where crystallization begins, T is the temperature at the time t. C is the cooling rate and dH is the heat flow determined from the DSC curves. The relative degree of crystallinity as a function of temperature for the PTT and PTT/ MWCNT (PTT-1.0) composite at different cooling rates is shown in Figure 7. It can be seen that all the curves have

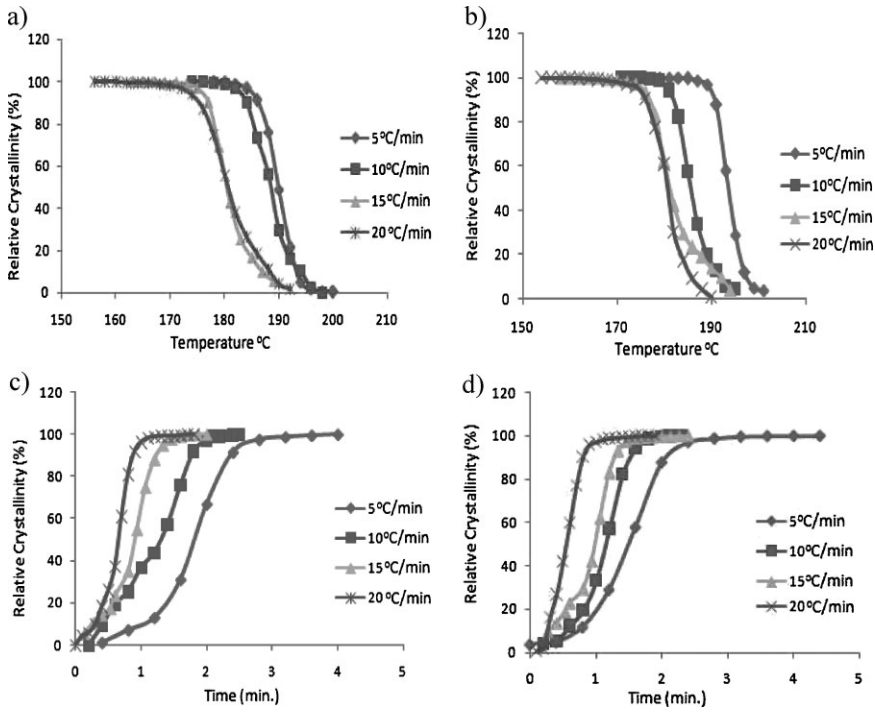

Figure 7.
Relative degree of crystallinity in PTT and PTT/MWCNT nanocomposites as a function of temperature and cooling rate.

Table 4.
Non-isothermal crystallization kinetic parameters of PTT/MWCNT nanocomposites.

Sample Designation	T_p (°C)	Cooling rate (°C)	n	k/sec^{-n}	$t_{1/2}$/min
PTT	190	5	3.8	1.8×10^{-2}	2.58
	185	10	3.0	7.6×10^{-1}	0.96
	181	15	2.6	1.67	0.71
	179	20	2.4	2.15	0.62
PTT-0.5	190	5	3.3	7.4×10^{-2}	1.95
	185	10	2.5	7.6×10^{-1}	0.96
	182	15	2.1	1.58	0.67
	178	20	2.3	2.13	0.61
PTT-1.0	189	5	3.3	8.8×10^{-2}	1.85
	185	10	2.4	7.2×10^{-1}	0.98
	181	15	2.0	1.43	0.69
	178	20	2.2	2.58	0.55
PTT-2.0	190	5	3.4	8.3×10^{-2}	1.85
	185	10	2.4	7.9×10^{-1}	0.95
	181	15	2.0	1.37	0.71
	179	20	2.1	2.29	0.56

sigmoidal shape and the crystallization occurred at lower temperature with increasing cooling rates, indicating that at lower cooling rates there is sufficient time to activate nucleation at higher temperatures. Figure 7 show that the time taken for complete crystallization decreased with increasing cooling rate. The values for the peak temperature (T_p), rate constant (k) and the crystallization half time ($t_{1/2}$) obtained from the non-isothermal crystallization traces of the PTT/MWCNT nanocomposites at different cooling rate are shown in Table 4.

It can be seen that the $t_{1/2}$ values for PTT and PTT/MWCNT nano-composites decreased with increasing cooling rate, indicating that higher the cooling rate, shorter the time for the crystallization. In addition for given cooling rate, the T_p values for PTT/MWCNT nanocomposites remain unchanged while $t_{1/2}$ values are lower only at lower cooling rate, whereas at higher cooling rate significant change was not observed. Therefore incorporation of MWCNTs in PTT induced nucleation only at lower cooling rate however at higher cooling rate CNTs didn't induce crystallization. Similarly, the rate of crystallization (k) of PTT/MWCNT nano-composites is also increasing with the addition of CNTs at lower cooling rate, indicating the acceleration of PTT crystallization upon incorporation of CNTs. Whereas at higher cooling rates, rate of crystallization is lower. Decrease in 'n' value can be attributed to the fact that in non-isothermal crystallization, time taken by the samples for the crystallization is very less as compared to isothermal process, since very small time is given for crystallization. Therefore, complete crystallization does not take place and leads to the formation of smaller spherulites. In addition, with increasing CNT content, 'n' value is decreasing, this shows that carbon nanotubes are hindering the chain mobility of polymer, which lead to the formation of smaller spherulites and this effect increases with increasing CNT loading.

Morphology of PTT/MWCNT composites was studied using PLM. Figure 8 show the PLM micrographs of PTT and PTT/MWCNT nanocomposites which support the results obtained from the isothermal DSC analysis. Micrographs show that small spherulites are observed for neat PTT matrix and the spherulitic size increased upon incorporation of MWCNTs, indicating that MWCNTs decreases the number of nucleating sites in the PTT matrix. These results revealed that MWCNTs hindered the chain mobility of polymer and decreased the heterogeneity therefore

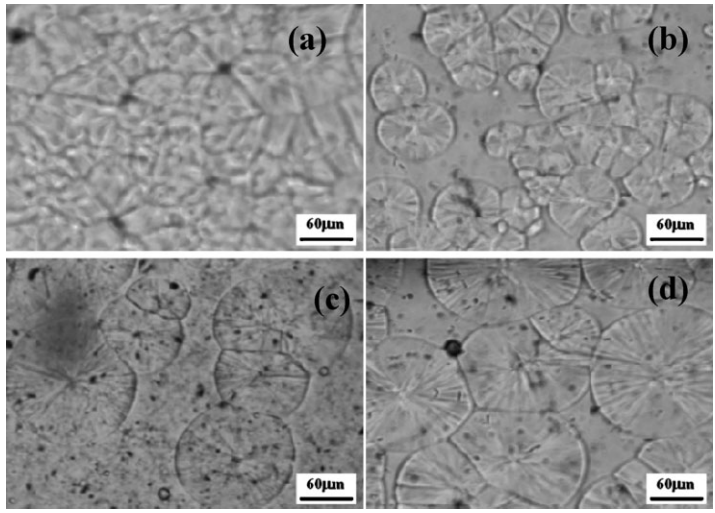

Figure 8.
PLM micrographs of PTT/MWCNT nanocomposites (a) PTT (b) PTT-0.5 (c) PTT-1.0 (d) PTT -2.0 after annealing time of 2 minutes at 200 °C.

leading to the formation of larger and more perfect spherulites.

Figure 9 show the effect of annealing time on spherulitic growth of polymer. It is well known from the literature that as annealing time increases the size of crystal increases and rate of crystallization decreases. PLM micrographs were taken at a time interval of 2 min at isothermal temperature of 200 °C. The size of spherulite increased with increasing annealing time. No change in spherulite size was

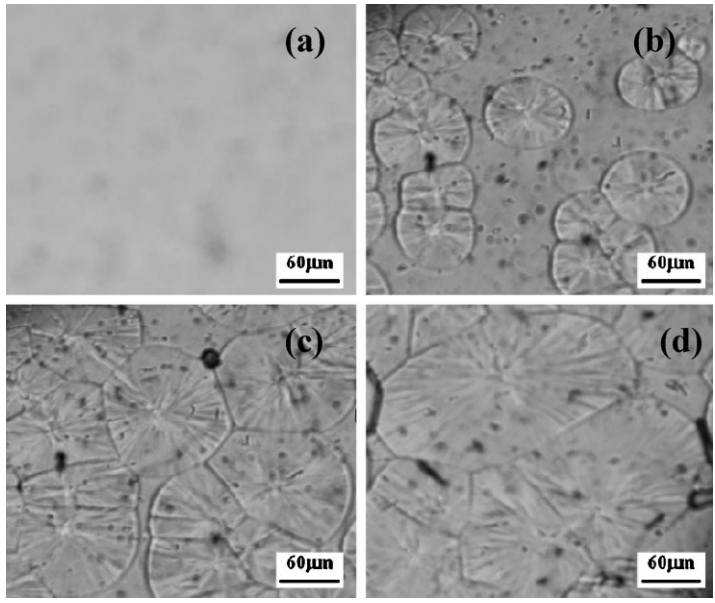

Figure 9.
PLM micrographs of PTT/MWCNT (PTT-0.5) showing effect of annealing time (a) 0.0 min (b) 2.0 min (c) 4.0 min (d) 6.0 min at 200 °C.

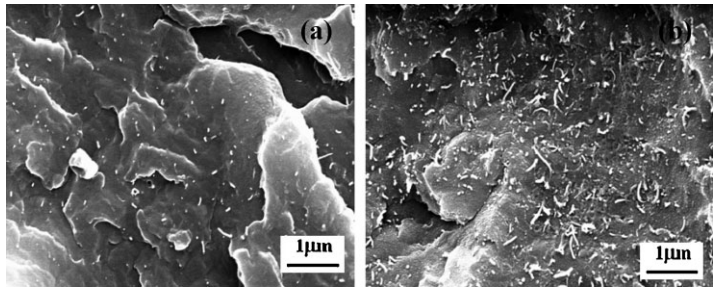

Figure 10.
SEM images of PTT/MWCNT nanocomposites (a) PTT-0.5 (b) PTT-2.0.

observed after 6 minutes of annealing time, this shows that longer time is required for complete crystallization at 200 °C. Higher rate of crystallization was found at lower isothermal temperature as compared to higher isothermal temperature therefore it was difficult to see the effect of annealing time at lower crystallization temperature as the time required for complete crystallization is less than one minute.

The SEM micrographs of PTT/MWCNT nanocomposites are shown in Figure 10. These images clearly show the uniform dispersion of nanotubes in the PTT matrix up to 2% (w/w) of MWCNTs. Nanotubes were found highly curved, randomly coiled and agglomerated because of the intrinsic vander Waals attractions between the individual nanotubes in combination with high aspect ratio and large surface area. Some CNT bundles were pulled out from the PTT matrix and some of the nanotube bundles were individually dispersed in the polymer matrix. Presence of pulled out nanotubes on the surface of nanocomposites showed poor interaction between CNTs and polymer matrix. TEM image of PTT nanocomposite containing 2 wt % of CNTs showed the presence of well dispersed [Figure 11(a)] and highly entangled CNTs [Figure 11(b)] in the polymer matrix. Figure 11(a) also showed that during compounding some of the nanotube bundles were opened and individually dispersed in the polymer matrix as diameter of nanotubes after compounding is same as the diameter of carbon nanotubes before compounding.

Figure 12(a) show the XRD patterns of PTT in the absence as well in the presence of varying amounts of MWCNTs. The characteristic XRD peaks for PTT were observed at 2θ of 15.7, 17.2, 19.6, 21.9, 23.7, 25.1 and 28.1° which correspond to the

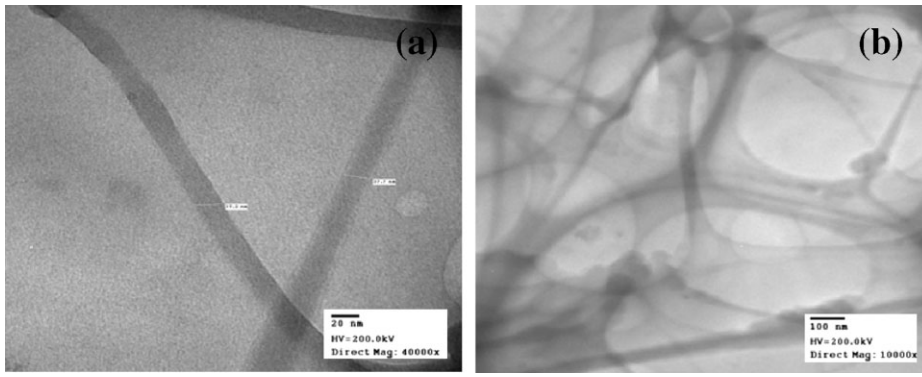

Figure 11.
TEM images of PTT/MWCNT nanocomposites.

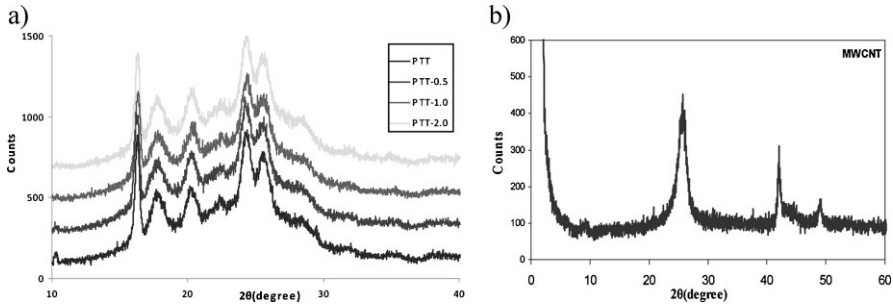

Figure 12.
XRD spectra of (a) PTT/MWCNT nanocomposites and (b) MWCNTs.

diffraction planes of (010), $(0\bar{1}2)$, (012), (102), $(1\bar{1}3)$, and $(1\bar{0}3)$, respectively. Two characteristic peaks were observed in XRD diffractograms of MWCNTs [Figure 12(b)] at 2θ of 27 and 43° which correspond to the diffraction planes of (002) and (101) respectively.[28] XRD spectra of nanocomposites show the characteristic pattern of virgin PTT, indicating that there is no change in crystal morphology of PTT upon incorporation of MWCNTs.

Based upon the diffraction pattern, the crystallite dimensions, L_{hkl} was calculated by using Scherrer equation [29]:

$$L_{hkl} = K\lambda/\beta_{hkl}\cos\theta_{hkl} \quad (6)$$

Where L_{hkl} is crystallite dimension perpendicular to the $(_{hkl})$ planes, K is the Scherrer constant and its value is taken as 0.9, λ is the wavelength of the X-rays, θ is the Bragg angle and β_{hkl} is the diffraction half width. The results are summarized in Table 5.

The crystallite dimensions (L_{hkl}) of PTT/MWCNT composites corresponding to $(0\bar{1}2)$, (012), planes are smaller than that of neat PTT whereas L_{hkl} for (010), $(1\bar{0}2)$, (102), $(1\bar{1}3)$ planes remain unchanged and a significant increase was observed in L_{hkl} for $(1\bar{0}3)$ planes upon addition of CNTs. However incorporation of CNTs didn't show any change in 2θ (Bragg angle) values. Since incorporation of CNTs didn't affect the crystal planes of PTT, however the crystal size of PTT in certain planes did change [Table 5]. Thus we can say that crystal size of PTT is affected by the incorporation of MWCNTs.

Figure 13 show the Raman spectra of pure PTT as well as PTT/MWCNT composites. In the Raman spectra of all the samples (PTT/MWCNT), peaks at 1290 cm^{-1} (assigned as D band and corresponds to disordered graphitic structure) and 1616 cm^{-1} (assigned as G band which correspond to the graphitic structure of carbon nanotubes) were observed. When the nanotubes are incorporated in the polymer, the polymer exert a pressure on individual nanotube increasing inter atomic distance of carbon atom in the nanotubes and thus vibrational frequency of some normal modes may change, causing a shift in G band. For samples having low concentration of CNTs, the quantity of PTT intercalated between nanotubes could lead to an opening of the bundles, enhancing the formation of nucleating agents to favor the crystallization process. On the

Table 5.
Results of XRD scans: Effect of MWCNTs on crystallite dimension of PTT.

Sample Designation	L_{010} (nm)	$L_{0\bar{1}2}$ (nm)	L_{012} (nm)	$L_{\bar{1}02}$ (nm)	L_{102} (nm)	$L_{11\bar{3}}$ (nm)	$L_{\bar{1}03}$ (nm)
PTT	3.0	3.5	4.3	3.5	4.5	4.5	2.3
PTT-0.5	3.0	3.0	3.5	3.3	4.5	4.5	3.3
PTT-1.0	3.0	3.5	3.5	3.2	4.5	4.5	3.0
PTT-2.0	3.0	3.0	3.5	3.2	4.5	4.5	3.0

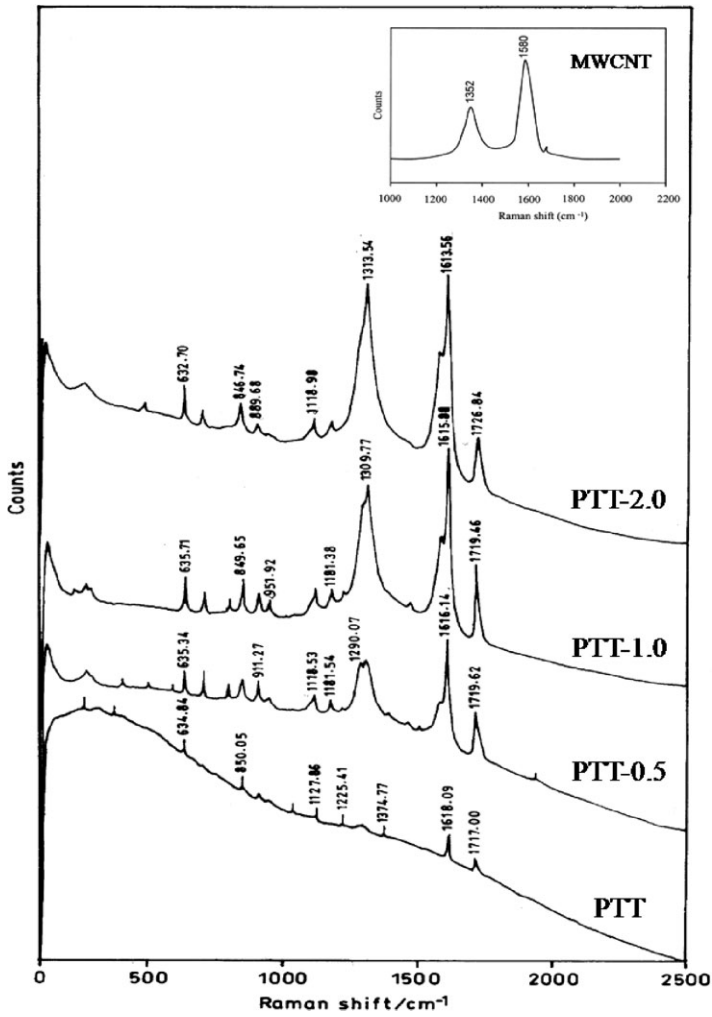

Figure 13.
Raman spectra of CNT and PTT/MWCNT nanocomposites.

other hand at higher nanotubes concentration, the nanotube bundles remain unopened and the quantity of aggregates increases with filler concentration keeping the polymer away from intercalation.

In the present work, no significant shift in G band was observed even at very small loadings of nanotubes which indicate that the nanotubes remain in the form of bundles and didn't act as nucleating agent. No shift in G band also indicates poor stress transfer between polymer and nanotubes due to the poor compatibility between these two as reported earlier.[30–32]

Conclusion

Incorporation of MWCNTs significantly affects the crystallization behavior of PTT. Non isothermal and isothermal crystallization experiments showed that incorporation of MWCNTs didn't affect the crystallinity of PTT and restricted the spherulitic growth of PTT. The nucleation sites decreased and spherical crystal size increased compared to neat PTT i.e carbon nanotubes reduced the transportation ability of polymer as well as facilitated the site to grow crystals. Therefore larger and more

perfect crystals were formed. Non-isothermal crystallization of PTT/MWCNT nanocomposites depended significantly on the MWCNTs content and cooling rate. Carbon nanotubes enhanced crystallization of PTT at lower cooling rate. PLM and Raman spectra also supported the DSC results. XRD studies showed that carbon nanotubes affected the crystal size of PTT. SEM and TEM results revealed that during compounding nanotube bundles were opened and individual nanotubes having diameter of 33–37 nm were seen dispersed in the polymer matrix.

Acknowledgements: University Grants Commission is gratefully acknowledged for providing financial assistance to one of the authors (Ms. Anju Gupta).

[1] Ouchi, M. Hosoi, S. Shimotsuma, *Appl. Polym. Sci.* **1977**, *21*, 345.
[2] H. Chuah, in: Modern Polyester, J. Scheirs, T. Long, (Eds.) Wiley, New York 2003.
[3] N. Dangseeyun, P. Srimoaon, P. Supaphol, M. Nithitanakul, *Thermochimi. Acta* **2004**, *409*, 63.
[4] J. M. Huanh, F. C. Chang, *Polym. Sci. Part B* **2000**, *38*, 934.
[5] J. R. Whinfield, J. T. Dickson, *British Patent* **1946**, *79*, 578.
[6] S. Wang, R. Liang, B. Wang, C. Zhang, *Chem. Phys. Lett.* **2008**, *457*, 371.
[7] G. Broaz, M. Kwiatkowaska, Z. Roslanies, K. Schulte, *Polymer* **2005**, *46*, 5860.
[8] M. Kwiatkowaska, R. Shearwood, P. Zchulte, *Polymer* **2000**, *46*, 5960.
[9] A. Cao, C. Lijie, G. Wu, B. Wei, C. Xu, J. Ling, D. Wu, *Carbon* **2001**, *39*, 137.
[10] X. Hu, A. J. Lesser, *Macro. Chem. Phys.* **2004**, *205*, 574.
[11] D. Wu, L. Wu, G. Yu, B. Xu, M. Zhang, *Polym. Engg. Sci.* **2008**.
[12] A. K. Anand, U. S. Agarwal, R. Joseph, *Polymer* **2006**, *47*, 3976.
[13] J. Y. Kim, S. Han, S. H. Kim, *Polym. Engg. Sci.* **2007**, *103*, 1450.
[14] J. Li, Z. Fang, Y. Zhu, L. Tong, A. Gu, F. Liu, *Appl. Polym. Sci.* **2007**, *105*, 3531.
[15] E. C. Chen, T. M. Wu, *Appl. Polym. Sci.* **2008**, *46*, 158.
[16] L. Valentini, J. Niagiotti, M. A. Lopez-Manchado, S. Santucci, J. M. Kenny, J. Appl, *Polym. Sci.* **2003**, *89*, 2657.
[17] A. Gupta, L. M. Manocha, V. Choudhary, *AIP. Conf. Proc.* **2008**, *1042*, 129.
[18] C. Wu, *Appl. Polym. Sci.* **2009**, *114*, 1633.
[19] Y. Xu, H. Jia, J. Piao, S. Ye, J. Haung, *J. Mater. Sci.* **2008**, *43*, 417.
[20] J. Y. Kim, H. S. Park, S. H. Kim, *Polymer* **2006**, *47*, 1379.
[21] R. B. Mathur, S. Seth, C. Lal, R. Rao, B. P. Singh, T. L. Dhami, *Carbon* **2007**, *45*, 132.
[22] K. Enomoto, S. Fujiwara, T. Yasuhara, H. Murakami, J. Tekari, N. Ohtake, *Jap. J. Appl. Phys.* **2005**, *44*, 888.
[23] P. Supaphol, N. Dangseeyun, P. Srimoaon, M. Nithitanakul, *Thermochemi. Acta* **2003**, *2*, 207.
[24] P. Srimoaon, N. Dangseeyun, P. Supaphol, *J. Euro. Polym. Sci.* **2004**, *3*, 599.
[25] M. Pyda, A. Boller, J. Grebowicz, H. Chuah, B. V. Lebedev, B. Wunderlich, *Polym. Phys. Part B* **1998**, *3*, 2499.
[26] Z. Li, G. Luo, F. Wei, Y. Huang, *Comp. Sci. Tech.* **2006**, *66*, 1022.
[27] J. Jin, M. Song, F. Pan, *Thermochimi. Acta* **2007**, *456*, 25.
[28] H. Liang, F. Guo, B. Chen, F. Luo, Z. Jin, *Polym. Bull.* **2008**, *60*, 115.
[29] D. Wu, L. Wu, G. Yu, B. Xu, M. Zhang, *Polym. Eng. Sci.* **2008**, *48*, 1057.
[30] J. Sandler, M. S. P. Shaffer, T. Prasse, W. Bauhofer, K. Sihutte, A. H. Windle, *Polymer* **1999**, *40*, 5967.
[31] L. S. Schadler, S. C. Giannairis, P. M. Ajayan, *Appl. Phys. Lett.* **1998**, *73*, 3842.
[32] J. Sandler, G. Broza, M. Nolte, K. Schulte, Y. M. Lam, M. S. P. Shaffer, *Macro. Sci. Part B* **2003**, *42*, 479.

